Shallow water channel estimation with energy efficient transmitted signal design

Naushad Ansari,[1] Ananya Sen Gupta,[2,a)] and Anubha Gupta[1]
[1]*Signal Processing and Bio-medical Imaging Laboratory (SBILab), Department of Electronics and Communication Engineering, Indraprastha Institute of Information Technology (IIIT)-Delhi 110020, India*
[2]*Department of Electrical and Computer Engineering, 4016 Seamans Center for the Engineering Arts and Sciences, University of Iowa, Iowa City, Iowa 52242, USA*

(Received 7 December 2017; revised 12 March 2019; accepted 23 March 2019; published online 16 May 2019)

This paper proposes channel estimation using energy efficient transmission of signal dictionaries for shallow water acoustic communications. Specifically, the multi-columned structure of the channel delay spread is exploited to design partially sampled dictionary in a two-dimensional (2-D) frequency representation of the channel. The key contribution of this work is to achieve considerable energy saving in the transmission of complex exponential signals, designed specifically for real-time shallow water channel estimation at the receiver. This is accomplished by harnessing 2-D frequency localization with compressive transmission and modified-compressive sensing with prior information to exploit the sparse structure of the rapidly fluctuating shallow water acoustic channel in real time. The proposed technique reduces demands on transmitted signal energy by harnessing the reconstruction ability of sparse sensing while retaining key non-sparse channel elements that represent important multipath phenomena. Numerical evidence based on experimental channel estimates demonstrates the efficacy of the proposed work. © *2019 Acoustical Society of America*.
https://doi.org/10.1121/1.5097581

[JFL] Pages: 2955–2970

I. INTRODUCTION

A fundamental challenge to shallow water acoustic communications and, hence, for autonomous underwater vehicles (AUVs), is robust real-time estimation of the rapidly time-varying underwater channel. The shallow water acoustic propagation channel manifests as a long delay spread, e.g., typically of about 4–16 ms in the channel impulse response. Further, the sparsity of the channel support is known to be time varying due to unpredictable shifts in the multipath arrivals. The time-varying sparsity is a challenge posed by the shallow water acoustic channel, which not only shows time variability across its delay taps due to multipath arrivals but also across the sparsity of its support. In particular, fluid motion, as well as time-varying multipath reflections from the moving sea surface, leads to rapid fluctuations in the channel impulse response, characterized by a highly time-varying and long delay spread.

Furthermore, unpredictable shifts in the underlying channel sparsity occur due to transient oceanic events such as surface wave focusing.[1] These oceanic phenomena as well as Doppler shifts, due to surface reflection and fluid motion, limit the reconstruction accuracy of most sparse recovery techniques. In particular, localization of non-stationary channel delay spread in time and frequency coupled with changing sparseness of channel support[2,3] renders direct application of sparse sensing methods challenging in the shallow water domain. This is particularly true under moderate to rough sea conditions when fluid motion and multipath channel effects are particularly pronounced and lead to high-energy transients that directly impact the sparsity of the underlying channel delay spread.[2,3] The performance of least-squares techniques has been analyzed in Ref. 4 in the context of random matrix theory. Such non-sparse techniques, if appropriately employed, can provide a complementary approach to shallow water channel estimation.

In the compressive sensing (CS) literature, the idea of compressive transmission is picking up pace where the central idea is that if full data can be recovered from the sensing of fewer data, it is better to transmit fewer data leading to compressive transmission that would save resources, including time and energy. Thus, compressive transmission leads to energy savings and, hence, is also called energy efficient transmission.[5–7] While this idea is being used in biomedical signal transmission,[5–7] it has not been introduced so far in the traditional acoustic communications. This concept may prove extremely useful for underwater communication scenarios. For example, submarines/AUVs used for defense purposes, in general, have limited power backup and are run on batteries. Using the proposed methodology, considerable energy can be saved by submarines/AUVs during transmission to the base station. Since base stations have sufficient energy and computational power, employing any advanced signal reconstruction method is not a challenge at the base station.

This motivated us to explore energy efficient dictionary transmission by transmitting dictionary elements (or basis functions) only on fewer sub-channels instead of all sub-channels. We harness a combination of compressive sampling, non-uniform frequency selection, and sparse

a)Electronic mail: ananya-sengupta@uiowa.edu

recovery techniques in the two-dimensional (2-D) frequency domain[8–10] to achieve energy efficient transmission for real-time channel estimation, and thereby, localize time-varying oceanic phenomena in the shallow water paradigm. The synopsis of the chosen channel model, related work, and key contributions are presented next.

A. Implications of energy efficient transmission

Given practical considerations of real-life underwater communication systems, energy efficiency is one of the many factors that need to be considered. However, robust communications is not the only goal of energy efficient channel estimation presented in this work. Energy efficiency for underwater signaling is an important consideration for low-energy oceanic observations, which is emerging as an important naval objective due to its potential for low-invasive and covert surveillance applications. In this regard, energy efficient channel estimation, due to its reduced average transmitted signal energy, can provide low-energy real-time interpretation of acoustic scatterers within the ocean environment. The problem of gleaning such information from the channel impulse response, although very interesting by itself, is a complex and active research question that falls outside the scope of this work, and the curious reader is directed to some preliminary work introduced in Refs. 11 and 12.

Compressive transmission by design employs drastically lowered transmitted signal energy by transmitting only a fraction of the overall encoding dictionary, and recovers the high-energy channel components using sparse optimization techniques. Through our results across channel simulations, as well as experimental field data, we demonstrate that channel estimation using compressive transmission allows such energy efficient observations of high-energy channel activity. For example, our compressive transmission technique employed across the 2-D frequency domain separates the high-energy steady-state aspects of the channel, e.g., the direct arrival, from transient and unpredictable high-energy events such as rapid multipath fluctuations. Such separation of different types of channel activity allows real-time interpretation of the shallow water acoustic channel using drastically lowered average transmission energy such as presented in this work.

B. Channel model: 2-D frequency characterization and sparsity of channel support

In this section, we adopt the 2-D frequency domain characterization of the shallow water acoustic channel introduced in Refs. 8–10, and use this representation for enabling energy efficient transmission of exponential signals for channel estimation. Specifically, we adopt transmission of signals over fewer subband channels leading to partial sampling of dictionary that *effectively* samples the shallow water channel in this representation non-uniformly, with 100% measurements or an effective denser (non-sparse) sampling along the steady-state channel components and sparse measurements along the transient channel components. We now elaborate on these separate channel components below.

The shallow water acoustic channel consists of primarily two types of temporally overlapping multipath phenomena: (i) high-energy transients and (ii) slowly varying channel components. Figures 1(a)–1(c) illustrate how these channel components manifest in different representations.

(i) High-energy transients in the channel activity: These can occur due to unpredictable oceanic phenomena such as constructive interference between different multipath reflections, surface wave focusing events, rapidly fluctuating scattering events, among others. The key characteristic of these channel components is that they manifest as the non-stationary or "transient" component of the shallow water acoustic channel along the higher Doppler frequencies. These high-energy yet ephemeral events, therefore, contribute to the sparse structure of the channel and can be best estimated using sparse sensing techniques such as[13–15] those that optimize toward finding the "outliers," i.e., the high-energy channel components.

(ii) Steady-state or slowly varying channel components: These occur due to the direct arrival from the transmitter to the receiver, as well as the relatively steady specular multipath reflections and diffused reflections from rough sea bottoms. These channel components constitute the "steady-state" part of the shallow water acoustic channel that needs to be observed over longer periods of time for precise estimation. These are best recovered by traditional least-squares techniques.[16,17] We note that slowly varying channel components may themselves be high-energy, e.g., the direct arrival from transmitter to receiver. The support of these channel components may or may not be sparse and depends on the channel representation. For example, in the delay vs time representation in Fig. 1(a), the direct arrival manifests as the long bright line at the bottom, whereas in the delay-Doppler channel representation in Fig. 1(b), the direct arrival shows up as a single bright dot at zero-Doppler frequency.

C. Justification for channel representation

2-D frequency representation allows us to effectively measure non-uniformly over the diverse channel components where (i) for the steady-state channel components, regardless of whether they are high- or low-energy and regardless of whatever sampling rate they are picked up, non-sampled measurements in the current time window are filled up with the immediately previous time windows' estimate (as noisy measurements) because of being the steady-state component. This leads to an effective sampling rate of 100% for steady-state channel components, and (ii) the transient components, which manifest in the outer columns, are measured (effectively) at lower sampling rates in comparison to the steady-state channel component. Support-constrained sparse recovery is employed to capture only the high-energy transient components. Other channel representations, such as the delay-Doppler representation, do not offer this type of

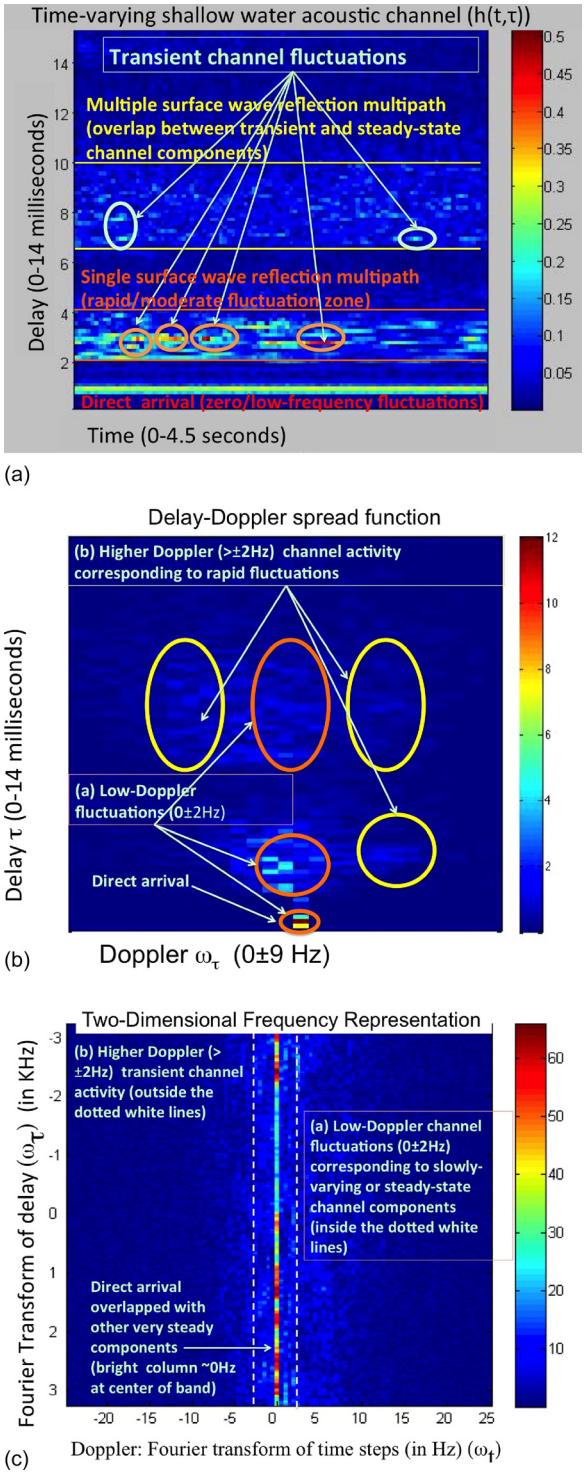

FIG. 1. (Color online) (a) Delay (τ) vs time (t) channel representation. (b) Delay (τ) vs Doppler (Ω_t) channel representation. (c) 2-D frequency channel representation: Delay frequency (Ω_τ vs Doppler Ω_t).

separation between the steady-state/persistent channel components and transient channel components.

The channel model corresponding to the 2-D frequency representation dissects all channel activity into slowly varying and/or steady-state components and rapidly fluctuating non-stationary components. Slowly varying multipath arrivals and quasi-stationary scattering events (e.g., diffused reflection from rocky bottom) tend to persist longer over time and, therefore, may be considered as the steady-state component of the channel that dominates the low-Doppler regions of the 2-D frequency characterization. However, high-energy transients due to unpredictable oceanic phenomena, such as constructive interference between different multipath reflections, surface wave focusing events, rapidly fluctuating scattering events, etc., manifest as non-stationary components or transient components of the shallow water acoustic channel along the higher Doppler frequencies.

We note that the 2-D frequency representation allows this separation of the steady-state and transient components of the channel more robustly than the delay-Doppler representation. The reasoning behind this is as follows.

The direct arrival and the slowly varying channel delay components occupy a single bright column at zero- and low-Doppler (± 1 Hz) in the 2-D frequency representation (with the Fourier transform in both the delay and time domains). *There is a very important distinction between this representation and the traditional delay-Doppler representation as the latter only takes the Fourier transform along the time domain and, thus, the energy at the really slowly varying or quasi-constant delay taps (e.g., due to the direct arrival) is smeared out across the* Ω_τ *domain, which is the Fourier transform along the delay domain* (since Fourier transform of an impulse, e.g., due to the direct arrival, will be a constant at all frequencies in the frequency domain). Thus, although the slowly varying components occupy the low-Doppler frequencies in the delay-Doppler domain similar to the 2-D frequency domain, they typically do not occupy distinct and different columns in the second dimension unlike as in the 2-D frequency domain. From a partial sampling perspective this means that it is more challenging to identify the support τ_c in the delay-Doppler domain than in the 2-D frequency domain.

D. Simulation evidence of adopted channel representation

We now provide two separate channel simulations using the well-known channel simulator[18,19] to provide justification for adopting the 2-D frequency domain as our preferred channel representation in this work. Figures 2 and 3 represent two independent implementations of the shallow water acoustic channel: (i) Fig. 2 shows the 2-D frequency representations of a calm channel with less multipath activity and transient scattering events, and (ii) Fig. 3 shows the 2-D frequency representations of a rough channel with increased multipath activity and higher intensity of transient scattering events. We observe that the second channel in Fig. 3 indeed exhibits more activity spread across higher Doppler frequencies (e.g., bright spots at -2 Hz) and wider support for Doppler activity (± 2 Hz vs ± 1 Hz). This is to be expected as transient multipath activity due to the fact that time-varying specular reflections from the sea surface will manifest at higher Doppler frequencies than steady-state scattering due to sea bottom and channel activity from relatively time-invariant direct arrival. We further note that while both channels exhibit consistent activity along the columns representing the delay frequency, the rougher channel shows more

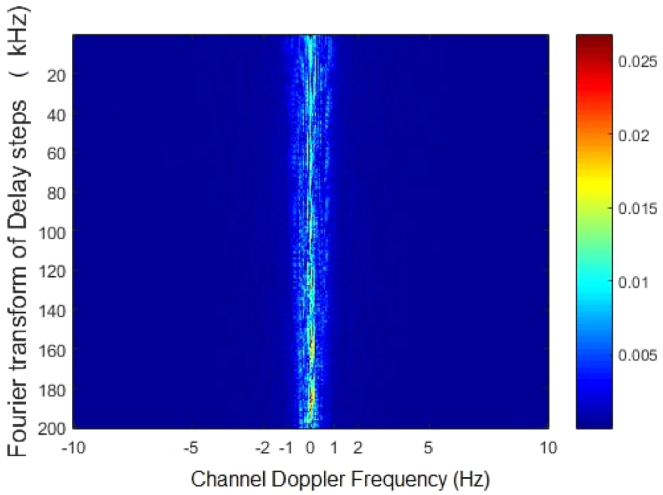

FIG. 2. (Color online) 2-D Fourier transform of a calm channel. Colorbar is linear.

spreading out of the channel support with more high-energy peaks (bright red spots) away from the zero-Doppler line.

E. Related work

Several estimation methods have been suggested in underwater communications literature[13,20,21] to estimate these diverse slow and rapidly varying channel components. For example, recently in Ref. 20, a mixed-norm optimization technique has been proposed that trades-off accuracy of detection of sparse and non-sparse components by choosing the optimization parameter $\lambda \in [0,1]$ at a suitable operating point in the well-known Lasso metric[22]

$$\mathbf{u}_{\text{opt}} = \arg\min_{\mathbf{u}} \left[(1-\lambda)\|\mathbf{u}\|_1 + \lambda \|\mathbf{C}\mathbf{u} - \mathbf{y}\|_2^2 \right], \tag{1}$$

where $\mathbf{u}$ denotes channel components to be estimated, $\mathbf{C}$ denotes the estimation matrix, and $\mathbf{y}$ denotes the received signal vector. However, such trade-offs typically lead to compromise in accuracy over high-energy transients while suppressing robust recovery of the diffused multipath delay spread from the sea bottom, in agreement with the three-way uncertainty relating time, frequency, and sparsity articulated in Ref. 3.

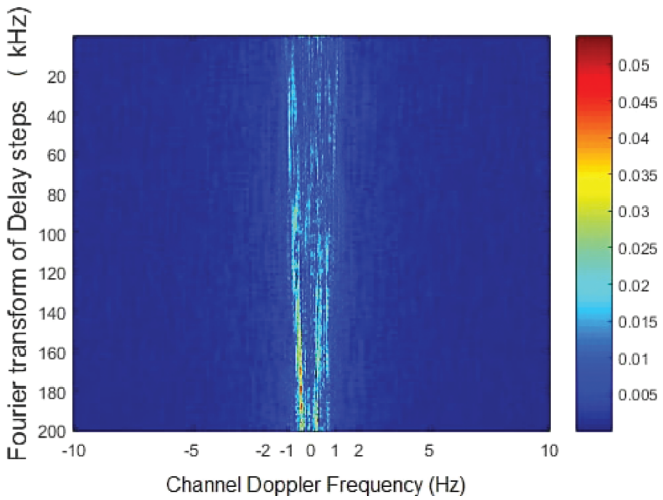

FIG. 3. 2-D Fourier transform of a rough channel. Colorbar is linear.

Unrelated to these channel estimation efforts using sparse sampling constraints, wireless communications, in general, has seen advances in orthogonal frequency domain multiplexing (OFDM) techniques[23–26] that also sample the channel in frequency domain. In OFDM, the channel is estimated by transmitting a few pilots, akin to compressive transmission. However, compressive transmission introduced in this work differs from the conventional OFDM systems, as well as traditional compressive transmission, in three significant ways:

1. Different pilot structure

In pilot based channel estimation, signal transmission would be done for a fixed number of pilots anchored at fixed positions across the channel frequency spectrum. In terms of shallow water acoustic channel, this means that OFDM pilots sample Doppler frequencies either at the pre-specified frequencies or according to some deterministic adaptive schemes. The compressive transmission scheme adopted in this work samples non-uniformly in a randomized (non-deterministic) manner across the Doppler frequencies. Since the column of zero-Doppler is the dominant channel component, we fill up the samples of zero-Doppler that are not sampled in the current time window with the estimates from the previous window assuming them to be the noisy measurements, yielding effectively a larger number of measurements for the zero-Doppler compared to the higher Doppler columns. A better estimate of channel is recovered with this strategy as elaborately discussed and shown in Sec. IV A.

2. Channel-cognizant localization

We exploit the relative localization of diverse channel components within the 2-D frequency representation, as discussed in detail in Secs. I C and I D, to design the sampling scheme based on the underlying physical phenomena that dominate the channel. As illustrated in Figs. 2 and 3, depending on the channel conditions (e.g., calm or rough), steady-state direct arrival and multipath scattering, highly transient multipath and focusing events, and other scattering, reflective, and interference phenomena manifest as moderate to high-energy channel components that exhibit varying sparsity of local support across the different Doppler columns. To the best of our understanding, popular OFDM[23] and popular compressive transmission methods[5–7] are completely agnostic of such physical phenomena.

3. Channel-adaptive energy efficiency

If the channel support itself is not highly time varying, i.e., the *contribution* from high-energy components along many Doppler columns does not rapidly fluctuate (even if the individual channel elements may vary rapidly), then the transmission scheme presented here can be adapted toward higher energy savings. Specifically, we can transmit even fewer dictionary atoms (equivalent to pilot reduction) saving transmit energy and fill-up the not-sensed or not-transmitted

samples of the steady-state components with the immediate prior time window's estimates, yielding an effective non-uniform measurements/sampling at different Doppler columns.

II. TECHNICAL APPROACH

A channel delay spread (∼30 ms long) of underwater acoustic channel estimated from field data collected at a depth of 15 m depth and 200 m range in the SPACE08 experiment[27] is shown in Fig. 1 as a function of time. From Fig. 1, two distinct arrival regions are noted to be present in the channel delay spread besides the dominant direct line-of-sight arrival. These are a primary multipath resulting from one or few reflections with sea surface,[3,13,20] and a secondary multipath resulting from several reflections between moving sea surface and bottom. With a significant contribution in channel energy and support, primary multipath delay taps are highly transient in nature and also exhibit high-energy peaks occasionally, as highlighted in Fig. 4, due to surface wave focusing[1] and other oceanographic events. The contribution of secondary multipath effects, while insignificant at the granularity of individual taps, cannot be ignored, and therefore cannot be suppressed at large. Hence, any transmitted signaling scheme needs to consider all three types of multipath effects (primary multipath, secondary multipath, and direct line-of-sight arrival), albeit in different ways.

Since the purpose of this work is to highlight how energy efficient compressive transmission can be harnessed in channel estimation, we employed the SPACE08 experimental data as a case study to demonstrate the key ideas of the paper. In addition, we have added more context and results with channels simulated by the well-know channel simulator[18,19] in Secs. I C and V B. This channel simulator has been proposed recently and is unrelated to the channel estimates of the SPACE08 experiment. This work does not make any comprehensive claim and, hence, does not require extensive validation on the utility of any channel or channel model. Also, the sparsity assumption for the channel support, while not universally true, is well documented to occur frequently. This provides support to the value added by this work.

III. DICTIONARY DESIGN AND POST-PROCESSING OF RECEIVED SIGNAL

In this section, we present transmitted signal dictionary design previously proposed in Refs. 8–10 and required for this work. Let us consider the dictionary elements (or basis functions) as complex exponential input signal $x[i,k] = e^{j2\pi ik/K}$ at time instant $i = 0,1,\ldots,L-1$ and delay frequencies $\omega_d = 0,2\pi/K,\ldots,2\pi k/K,\ldots,2\pi(K-1)/K$ with $k = 0,1,\ldots,K-1$ across K parallel sub-channels. Also, we consider Doppler frequencies $\omega_D = 0,2\pi/L,\ldots,2\pi l/L,\ldots,2\pi(L-1)/L$ with $l = 0,1,\ldots,L-1$. Let the channel impulse response be $h[i,n]$ at time instant i and channel delay tap $n = 0,1,\ldots,K-1$. The following signal is obtained on transmission of the signal $x[i,k]$ over the channel

$$y[i,k] = \sum_{n=0}^{K-1} h[i,n]x[i-n,k] = \sum_{n=0}^{K-1} h[i,n]e^{j2\pi(i-n)k/K} = e^{j2\pi ik/K}\sum_{n=0}^{K-1} h[i,n]e^{-j2\pi nk/K}. \tag{2}$$

On multiplication with $e^{-j2\pi nk/K}$ on both sides of Eq. (2), we obtain

$$y[i,k]e^{-j2\pi ik/K} = \sum_{n=0}^{K-1} h[i,n]e^{-j2\pi nk/K}. \tag{3}$$

On computing the one-dimensional Fourier transform along the time variable i in Eq. (3) leads to

$$U[l,k] = \sum_{i=0}^{L-1} y[i,k]e^{-j2\pi ik/K}e^{-j2\pi il/L} \tag{4}$$

$$= \sum_{i=0}^{L-1}\sum_{n=0}^{K-1} h[i,n]e^{-j2\pi nk/K}e^{-j2\pi il/L}. \tag{5}$$

This is to note that Eq. (5) represents the 2-D Fourier transform of the channel impulse response $h[i,k]$ and, hence, can be rewritten in the matrix form as

$$\mathbf{U} = \mathfrak{F}\mathbf{H}, \tag{6}$$

where $\mathbf{U}$ is the matrix representation of $U[l,k]$ with dimension $L \times K$. $\mathfrak{F}$ denotes the 2-D Fourier transform operator and $\mathbf{H}$ of size $L \times K$ is the matrix representation of the channel impulse response $h[i,n]$. From Eq. (6), it is clear that the post-processed received signal $\mathbf{U}$ corresponds to the 2-D Fourier transform of the channel. Figure 5 represents the 2-D

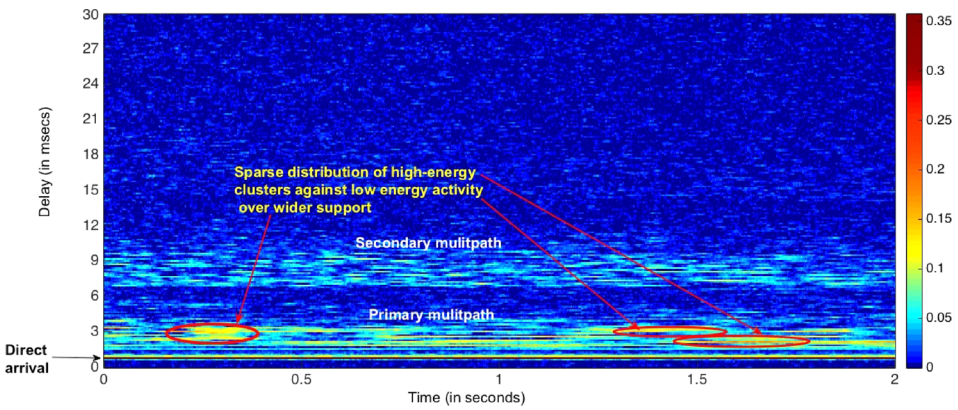

FIG. 4. (Color online) Delay spread (y axis) plotted at different time instants (x axis). Color intensity at any point represents delay tap magnitude. Colorbar is linear.

Fourier transform of the channel shown in Fig. 4. Note that the Doppler frequencies are shown on the x axis in Fig. 5 or the rows of $\mathbf{U}$ and delay frequencies are along the y axis in Fig. 5 or columns of $\mathbf{U}$.

From Eq. (6), we observe that, in the noise free scenario, the channel can be recovered by computing the 2-D inverse Fourier transform of the post-processed received signal $\mathbf{U}$. Thus, the proposed dictionary design transmission and post-processing of the received signal has transformed the problem of channel estimation in the time-domain to recovery of channel from the Fourier domain.

Interestingly, this framework is similar to k-space based image reconstruction in magnetic resonance imaging (MRI) where the CS approach is extensively used.[28,29] Motivated with this, we used CS and modified-CS based approaches with prior information in the above framework for underwater channel estimation in Ref. 10. However, energy efficient transmission was not considered in Ref. 10, which is the focus of the current work and is described in Sec. IV.

IV. ENERGY EFFICIENT DICTIONARY TRANSMISSION—PARTIAL TRANSMISSION OF DICTIONARY ELEMENTS

This section presents energy efficient partial transmission that builds on the channel estimation framework introduced in Ref. 10. From an energy efficiency perspective, higher frequency transients typically occupy less energy than the direct arrival $U[0,k]_{k=0}^{K-1}$ and, therefore, the input signal dictionary can be designed to detect more activity around the direct arrival and primary multipath region, with partial sampling along the secondary multipath region. The trade-off between energy efficiency and performance will be assessed by the relative performance margins of the sampling ratios chosen.

Compressive transmission and sampling ratio: Compressively transmitting the data for the purpose of channel estimation in this study is equivalent to transmitting the designed dictionary atoms over a few delay subcolumns. Consider Eq. (5) where K possible delay frequencies $\omega_d = 0,2\pi/K,\ldots,2\pi(K-1)/K$ based input dictionary elements of complex exponential $x[i,k] = e^{j2\pi ik/K}$ are required to be transmitted across K parallel sub-channels. Let us assume that only $S_r\%$ (S_r represents sampling ratio in percentage) of dictionary elements (or basis functions) are transmitted, i.e., K' sub-channels are selected randomly, where $K' = \lfloor K \times S_r/100 \rfloor$. In other words, if $\Omega = \{0,1,\ldots,K-1\}$ is the set of indices of all delay frequencies, it is assumed that Ω_s is a subset of these indices, i.e., the set of indices of randomly selected sub-channels with $\Omega_s \subseteq \Omega$, where $|\Omega| = K$, $|\Omega_s| = K'$, and $|\cdot|$ denotes the cardinality of the set. In terms of matrix representation, a sampling ratio of $S_r\%$ implies that $S_r\%$ of rows of channel $\mathbf{U}$ shown in Fig. 5 are fully transmitted to the receiver.

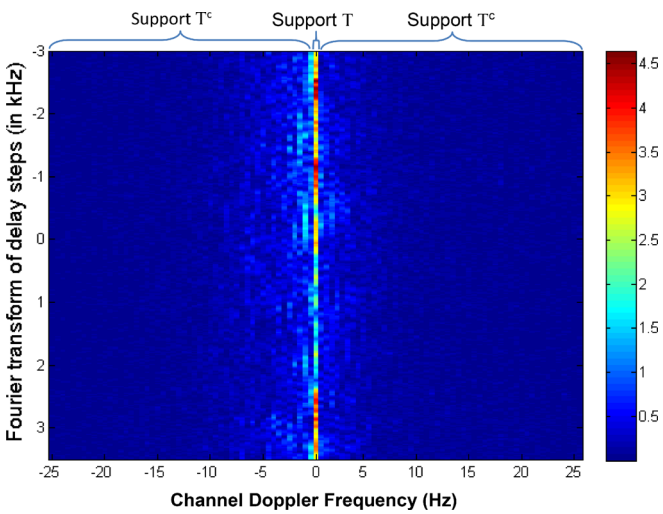

FIG. 5. (Color online) 2-D Fourier transform of the channel shown in Fig. 4. Colorbar is linear.

Channel estimation: On carrying out post-processing similar to Eq. (5), we can rewrite Eq. (6) for energy efficient transmission as

$$\mathbf{U}_{\text{sub}} = \Re\mathfrak{F}\mathbf{H}, \tag{7}$$

where $\Re$ is the operator denoting the restriction operator on $\mathfrak{F}\mathbf{H}$ and is an equivalent representation of transmitting fewer dictionary atoms or exponential signals. Hence, $\mathbf{U}_{\text{sub}}$ in Eq. (7) can be represented in terms of $\mathbf{U}$ in Eq. (5) with the following relation:

$$\mathbf{U}_{\text{sub}} = O(\mathbf{U}), \tag{8}$$

where O is the operator that transfers the post-processed signal $U[l,k]$ only at delay frequencies $2\pi k/K = 2\pi k_s/K$ and transfers nothing at delay frequencies $2\pi k/K \neq 2\pi k_s/K$, where $k_s \in \Omega_s$. In matrix form, the above relation can be written as

$$\mathbf{U}_{\text{sub}} = \Re\mathbf{U}, \tag{9}$$

where $\Re$ is an operator that represents selection of fewer columns from the matrix $\mathbf{U}$. $\mathbf{U}_{\text{sub}}$ has dimension $L \times K'$, where $K' \leq K$ and is the post-processed received signal when input is transmitted across selected sub-channels only.

The received signal in a noisy channel is represented by

$$\mathbf{U}_{\text{sub}} = \Re\mathbf{U} + \mathbf{N}, \tag{10}$$

where $\mathbf{N}$ is the complex white Gaussian noise matrix with dimension $L \times K'$. The post-processed received signal $\mathbf{U}$ can be estimated from the observed $\mathbf{U}_{\text{sub}}$ by solving the following LASSO (least absolute shrinkage and selection operator)[22] optimization problem:

$$\tilde{\mathbf{U}} = \arg\min_{\mathbf{U}} \|\mathbf{U}_{\text{sub}} - \Re\mathbf{U}\|_F^2 \ \text{ subject to } \|\mathbf{U}\|_1 \leq \tau, \tag{11}$$

where τ is the measure of sparsity of $\mathbf{U}$. Here, $\|\cdot\|_F^2$ represents the square of the Frobenius norm and is equal to the sum of squares of entries of the matrix, and $\|\cdot\|_1$ represents the l_1-norm given by the sum of absolute values. From Fig. 5, it is noted that the zero-Doppler frequency or the center column of $\mathbf{U}$ corresponds to the invariant or the most dominant steady component of the channel and, hence, contains

most of the energy. The steady-state components can also include slowly varying multipath scattering, which will occupy the low-Doppler frequencies around ± 1–1.5 Hz. On the other hand, higher Doppler frequencies contain relatively less energy and are sparser than the zero-Doppler frequency component. Since the low-Doppler frequency components are the most dominant components, they may lead to a better estimate of $\mathbf{U}$ if known *a priori*. From Eqs. (3) and (4), we observe that data are received for some of the components of zero-Doppler frequency, particularly, $U[0,k]$ where $k \in \Omega_s$. On the other hand, data are not received for $k \notin \Omega_s$ at the receiver with the compressive transmission, i.e., $U[0,k]$ with $k \notin \Omega_s$ is not received. Assuming comparatively less change in the low-Doppler frequency component from one time window to another, we consider the prior window estimate of the unknown (not measured) components $U[0,k]$ with $k \notin \Omega_s$ as the current window's noisy measurements, i.e.,

$$U_j[0,k]_{k\notin\Omega_s} = U_{j-1}[0,k]_{k\notin\Omega_s} + \eta, \tag{12}$$

where $U_j[l,k]$ and $U_{j-1}[l,k]$ are the jth and $(j-1)$st window estimates of the post-processed received signal, respectively, and η is the noise that represents change in $U[0,k]_{k\notin\Omega_s}$ between two consecutive windows. With the above formulation of Eq. (12), we have samples of zero (or low) Doppler at all delay frequencies, while we have measured data for other Doppler frequencies ($l \neq 0$) at only sampled/transmitted delay frequencies belonging to Ω_s, i.e., we have received $U[l,k]_{l\neq 0, k\in\Omega_s}$ in the post-processed received signal for the current observation window only.

Instead of directly translating classic range rate and path length fluctuations to specific Doppler subbands, our motivation is to broadly separate the channel into mutually exclusive supports, T and T^c (refer to Fig. 5). Each Doppler frequency column consists of all delay frequencies $k \in \Omega_s$ in the 2-D channel representation corresponding to the particular Doppler frequency. T represents the low-Doppler columns that capture the steady-state/slowly varying components of the channel, which do not follow a sparse distribution, and T^c represents the transient channel components, which do follow a sparse support. This implies that the zero- (or low-) Doppler (center columns of $\mathbf{U}$), corresponding to the non-sparse support T, should be fully measured, i.e., no partial sampling should be done. However, we perform compressive measurements, i.e., less than 100% sampling of the channel. Thus, in order to capture all data points of zero-Doppler (support T), we fill-up the non-measured data points of the zero-Doppler in the current window with the estimates of the previous window because these are slow varying data points across time windows. This leads to an effective 100% sampling of zero-Doppler (although noisy) and sampling of fewer data points along Doppler frequency columns corresponding to the sparse support T^c. Each channel estimate with this non-uniform sampling scheme [full (effective) sampling at low-Doppler columns and partial sampling at higher Doppler columns] is updated in every observation window, with j being the window index, as shown in Eq. (10). For notational simplicity, we henceforth drop the window index subscript j since the channel would be estimated for every window in a similar fashion.

To summarize mathematically, it is observed from Fig. 5 that $\mathbf{U}$ is not sparse on its full support but only on the support T^c. $\mathbf{U}$ is observed to be dense on the support T. Hence, it is more appropriate to impose sparsity only on the support T^c instead of imposing it on the full support of $\mathbf{U}$. Based on this, the optimization problem of Eq. (11) is reformulated as

$$\tilde{\mathbf{U}} = \arg\min_{\mathbf{U}} \|\mathbf{U}_{\text{sub}} - \Re\mathbf{U}\|_F^2 \ \text{ subject to } \ \|\mathbf{U}_{T^c}\|_1 \leq \tau, \tag{13}$$

where $\mathbf{U}_{T^c}$ refers to the components of $\mathbf{U}$ belonging to support T^c. The above formulation is also known as modified-CS.[30] Equation (13) can be written in the vectorized form as

$$\tilde{\mathbf{u}} = \arg\min_{\mathbf{u}} \|\mathbf{u}_{\text{sub}} - \Re_v\mathbf{u}\|_2^2 \ \text{ subject to } \ \|\mathbf{u}_{T^c}\|_1 \leq \tau, \tag{14}$$

where $\mathbf{u}$ and $\mathbf{u}_{\text{sub}}$ are the vectorized forms of $\mathbf{U}$ and $\mathbf{U}_{\text{sub}}$, respectively, and the operator $\Re_v$ carries out the sampling in the vectorized form.

Next, we provide an explanation for solving Eq. (14). Note that $\|\mathbf{u}_{T^c}\|_1 = \|\mathbf{W}\mathbf{u}\|_1$, where $\mathbf{W}$ is the diagonal matrix with diagonal entries given by

$$W(i,i) = \begin{cases} 1 & \text{if } i \in T^c, \\ 0 & \text{otherwise.} \end{cases} \tag{15}$$

Hence, Eq. (14) can be written as

$$\tilde{\mathbf{u}} = \arg\min_{\mathbf{u}} \|\mathbf{u}_{\text{sub}} - \Re_v\mathbf{u}\|_2^2 \ \text{ subject to } \ \|\mathbf{W}\mathbf{u}\|_1 \leq \tau. \tag{16}$$

Now, let us consider $\mathbf{v} = \mathbf{W}\mathbf{u}$ or $\mathbf{u} = \mathbf{W}^{-1}\mathbf{v}$. This results in the following optimization problem

$$\tilde{\mathbf{v}} = \arg\min_{\mathbf{v}} \|\mathbf{u}_{\text{sub}} - \Re_v\mathbf{W}^{-1}\mathbf{v}\|_2^2 \ \text{ subject to } \ \|\mathbf{v}\|_1 \leq \tau. \tag{17}$$

Since $\mathbf{W}$ is a diagonal matrix, its inverse can be computed by simply computing the inverse of its diagonal elements. However, $\mathbf{W}$ is singular because some of its diagonal elements are zero. Hence, we modify the diagonal entries of $\mathbf{W}$ to make it invertible as shown by

$$W(i,i) = \begin{cases} 1 & \text{if } i \in T^c, \\ \epsilon & \text{otherwise,} \end{cases} \tag{18}$$

where ϵ is a small value close to zero that restricts the elements in $\mathbf{W}^{-1}$ from reaching infinity.

Equation (17) can be solved using any LASSO solver. Here, it is solved using MATLAB solver spgl1.[31,32] $\tilde{\mathbf{u}}$ is estimated as $\tilde{\mathbf{u}} = \mathbf{W}^{-1}\tilde{\mathbf{v}}$ after solving Eq. (17). All the steps for solving Eq. (14) are provided in Algorithm 1.

ALGORITHM 1: Algorithm to estimate channel using the proposed formulation.

Input: Sampled post-processed received signal $\mathbf{u}_{T^c}$ and operator $(\Re_v)$
Output: Full signal $(\tilde{\mathbf{u}})$

- Step 1: Form weight matrix $\mathbf{W}$ as explained in Eq. (18), and compute its inverse.
- Step 2: Solve:
$$\tilde{\mathbf{v}} = \min_{\mathbf{v}} \|\mathbf{u}_{\text{sub}} - \Re_v \mathbf{W}^{-1}\mathbf{v}\|_2^2, \quad \text{such that } \|\mathbf{v}\|_1 \leq \tau$$
using any solver for LASSO.
- Step 3: Compute $\tilde{\mathbf{u}}$ using $\tilde{\mathbf{u}} = \mathbf{W}^{-1}\tilde{\mathbf{v}}$ and obtain its matrix form $\tilde{\mathbf{U}}$.
- Step 4: Obtain estimated channel from $\tilde{\mathbf{U}}$ using Eq. (6), i.e., $\tilde{\mathbf{H}} = \tilde{\mathfrak{F}}^{-1}\tilde{\mathbf{U}}$.

A. Strategies to reuse estimates of zero-Doppler channel component

As discussed in Sec. IV, zero-Doppler denotes the steady-state component carrying higher energy data samples. Hence, all the data points of zero-Doppler are important to be sampled (or be known or received at the receiver) from the point of view of quality channel estimation. However, at a sampling ratio of $S_r\%$, only $S_r\%$ of rows of channel matrix $\mathbf{U}$ (Fig. 5) are being transmitted and, hence, only $S_r\%$ data points of the zero-Doppler (center column of channel matrix $\mathbf{U}$) are measured in the current time window. Since data points of zero-Doppler are important, samples of zero-Doppler that are not measured in the current window are filled up using the previous window's estimates as specified in Eq. (12), considering them as the noisy measurements of the present window, i.e., we re-use the estimates of zero-Doppler data points of previous window as the noisy sensed data in the current window at the receiver. However, this is only one of the possible methods to handle not-measured zero-Doppler data points. In this subsection, we present other possibilities or methods to fill zero-Doppler data points (which are not measured in the current window) for channel estimation. Comparison results of these methods will be presented in Sec. V to validate the appropriateness of the chosen method discussed in Sec. III. We present four possible methods that can be used on zero-Doppler samples:

(1) Method 1: The first method is the conventional method of CS where data points that are not measured/sensed in the CS scenario are considered to be zero and will be filled up only after the CS based reconstruction is applied, i.e., data points of zero-Doppler that are not measured in the current window are not filled-up with any *a priori* estimate. In other words, assume that $\mathbf{U}_j[0,k]_{k\notin\Omega_s} = 0$ is received at the receiver, where j is the index of the current window.
(2) Method 2: Assuming comparatively less change in the zero-Doppler frequency component from one time window to another, the prior window's estimates of all the data points of zero-Doppler are used as the noisy measurements of zero-Doppler in the current window, i.e., $U_j[0,k] = U_{j-1}[0,k] + \eta, \ \forall k \in [0, K-1]$, where η is the noise in zero-Doppler samples.
(3) Method 3: The prior window's estimates of only the unknown data points of zero-Doppler $U[0,k]$ (components not measured in the current window) with $k \notin \Omega_s$ are considered as the current window's noisy measurements as specified in Eq. (12). In this method, we fixed Ω_s for all the windows before the experiments. This implies that the compressive transmission is carried out over some fixed delay subcolumns ($k \in \Omega_s$) in all the successive time windows.
(4) Method 4: This is same as Method 3 except that Eq. (12) is used with variable Ω_s to fill up non-measured data points of zero-Doppler in successive time windows. This is the most practical case because it implies that the delay subcolumn channels are chosen randomly for compressive transmission of dictionary elements in different time windows for channel estimation.

B. Energy savings in transmitted signal from partial sampling

This is to note that if we consider energy required in the process of signal transmission for channel estimation, sending a few frequency components (via partial sampling along higher Doppler frequencies) provides energy saving in the process. For example, if a signal is transmitted at $S_r\%$ sampling ratio (or at $S_r\%$ sub-channels), it directly implies that $(100 - S_r)\%$ energy is saved in this process of signal transmission as compared to 100% sampling ratio, where the signal is transmitted at all sub-channels or when full dictionary is transmitted.

Thus, the metric for measuring energy savings is directly proportional to the sampling ratio, which has been used widely in the bio-medical signal processing community.[5–7] In applications related to data communication and channel capacity,[33,34] bits-per-joule is a relevant metric. On the other hand, this work is focused on channel estimation, where "transmission energy" savings simply refers to saving energy in the transmission of training symbols by sending far fewer symbols than in the traditional non-sparse dictionaries. The relevant metric in efficiency is, therefore, the sampling ratio and, hence, in all the above results, compressive transmission implies energy efficient transmission.

Following this point, full dictionary transmission or 100% sampling ratio implies no energy saving in the process of training symbol transmission. Hence, 100% sampling ratio is not of importance from the energy saving point of view, whereas a sampling ratio of $S_r\%$ ($S_r < 100$) implies (100 - S_r)% energy saving with slightly less reconstruction accuracy (refer to Figs. 7 and 8) compared to full dictionary transmission. Thus, there is a trade-off between channel reconstruction accuracy and energy saving. Better reconstruction accuracy implies less energy saving. Thus, one may go for full dictionary transmission with best channel reconstruction accuracy and no saving in energy or partial dictionary transmission with slightly less reconstruction accuracy and saving in energy.

V. RESULTS

Choice of the observation window length and sampling ratio localizes different channel activity in time and sparsity, i.e., captures different components of steady-state vs transient channel activity. Usually the high-energy channel

transients, being ephemeral, can only be localized using shorter observation windows, whereas the steady-state components are best captured in longer observation windows. Usually, for calm to moderate channels, high-energy transient activity is rare and unpredictable, and therefore, manifests within the very sparse support of the channel in the high-Doppler columns. On the other hand, rough channels that exhibit significant and frequent rapid fluctuations exhibit less sparse support in the high-Doppler columns. Accordingly, we expect better performance and, hence, more transmitted signal energy savings using compressive transmission for calm to moderate channels over rough or highly active channels. Accordingly, we provide results and relevant discussion over two independent sets of numerical experiments:

(i) Numerical results based on one real-world channel estimated from experimental field data conducted from October 18 to October 27 in 2008 (SPACE08 experiment).[27] The channel based on SPACE08 data is a moderately calm channel, hence, all results for this channel follow non-sparse channel activity at lower Doppler and sparse activity at high Doppler, and

(ii) numerical results based on a well-known channel simulator[18,19] to create a calm/moderate channel and a rough channel and show how the results change based on the channel conditions.

In each case, we discuss our numerical results based on trade-off between sparsity, observation window length, and choice of sampling ratio. We also provide performance studies of our method across channel simulations that vary the multipath, spreading factor, and bandwidth.

A. Numerical results based on experimental data

This section presents numerical results based on one experimental channel estimated from experimental field data conducted from October 18 to October 27 in 2008.[27] Mixed-norm optimization technique[20] is employed to sample the non-stationary channel at several points in time, spaced 100 ms apart (approximately one channel length). Figure 6 shows the channel impulse response estimated, using Ref. 20 from the above mentioned experimental data, as a function of time for 30 ms duration collected over moderate to rough sea conditions. From Fig. 6, it is noted that despite similar regions of activity, there is a noticeable distinction between the two temporal snapshots. These channel values are used as ground truth in the proposed formulation as discussed in Secs. III and IV. Thus, the channel considered in this section is not a simulated product of acoustic propagation models, but is the true (optimized for best normalized prediction error) estimate of a real channel over which the SPACE08 experiment was conducted.

The experiment of underwater acoustic channel estimation is performed with fewer randomly selected dictionary signal transmissions with received signal-to-noise ratios (SNR) of 10 dB and 5 dB (received over noisy channel). Accuracy of the proposed method of channel reconstruction

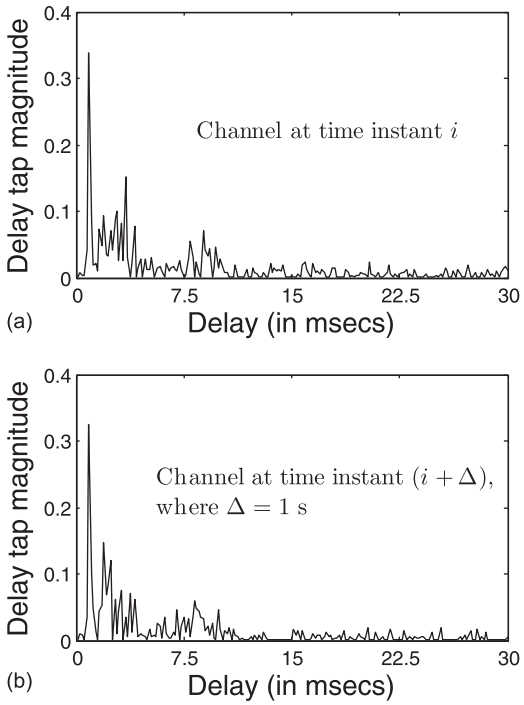

FIG. 6. Representative channel estimates at two different time instants over 30 ms delay using Ref. 20 as kernel solver.

is quantified in terms of normalized mean square error (NMSE) and is given by

$$\mathrm{NMSE\,(in\,dB)} = 10\log_{10}\left(\frac{\sum_{i=0}^{L-1}\sum_{k=0}^{K-1}|H(i,k)-\hat{H}(i,k)|}{\sum_{i=0}^{L-1}\sum_{k=0}^{K-1}|H(i,k)|^2}\right), \tag{19}$$

where $\mathbf{H}$ and $\hat{\mathbf{H}}$ represent the channel ground truth and reconstructed channel, respectively. The SNR of the noisy channel is given by the following relation:

$$\mathrm{SNR\ of\ noisy\ channel} = 10\log_{10}\left(\frac{\frac{1}{LK}\sum_{i=0}^{L-1}\sum_{k=0}^{K-1}|h(i,k)|^2}{\sigma_n^2}\right), \tag{20}$$

where σ_n^2 denotes the variance of noise present in the noisy channel.

Channel reconstruction results in terms of NMSE (in dB) are shown in Figs. 7 and 8 for noisy channel SNRs of 10 dB and 5 dB, respectively. The experiment is performed with sampling ratio ranging from 40% to 100% and with window length ranging from 0.92 ms (milliseconds) to 23.04 ms. As discussed in Sec. IV, we use the previous window estimate of zero-Doppler components of post-processed received signal (i.e., $\mathbf{U}[0,k]_{k\notin\Omega_s}$) to estimate the channel in the present window. Hence, the channel is estimated in 100 continuous non-overlapping windows and results are averaged over those 100 windows. Also, 50 Monte Carlo

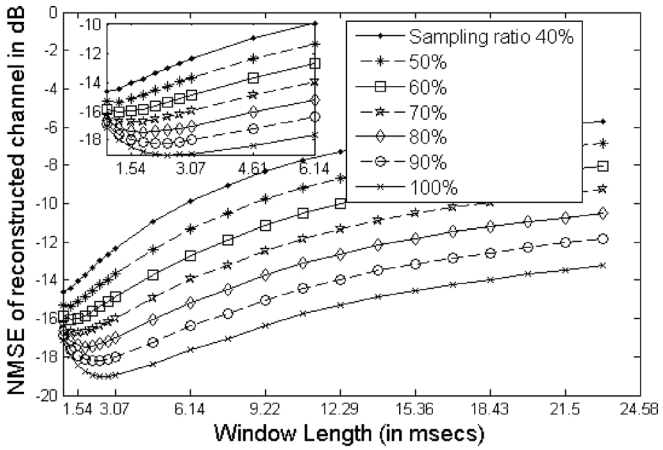

FIG. 7. NMSE for channel estimates using Ref. 17 with noisy channel SNR = 10 dB with modified CS recovery framework and transmission of dictionary elements over fewer frequency sub-channels; support T corresponds to the zero-Doppler component.

simulations of the above complete experiment are performed and results are shown in Figs. 7 and 8.

From Figs. 7 and 8, we observe that 100% sampling ratio, which represents the non-compressed dictionary or the full dictionary transmission, dominates the NMSE performance. Also, the performance decreases as the sampling ratio decreases. This is to be expected as ideally, 100% sampling across the full channel support, i.e., $T \cup T^c$ should capture the full channel activity. Moreover, as the sampling ratio decreases, we rely more on the previous window estimate for zero-Doppler frequency [refer to Eq. (12)], which is the most dominant component of the channel. Due to time-varying nature of the channel, this decreases the channel reconstruction accuracy and, hence, a corresponding increase in NMSE estimation error. However, despite achieving a lower estimation error, 100% sampling also implies no compression and, therefore, 0% energy savings in the transmitted signal. Hence, the goal is to study the trade-off between estimation error and sampling ratio, which is proportional to the transmitted signal compression, and thus, transmitted energy savings.

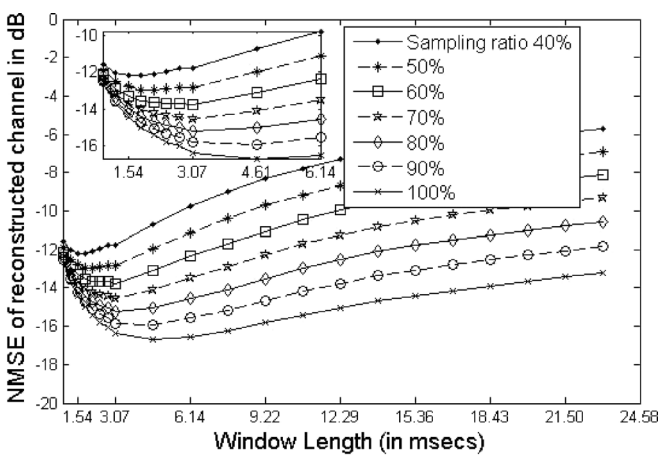

FIG. 8. NMSE for channel estimates using Ref. 17with noisy channel SNR = 5 dB with modified CS and transmission of dictionary elements over fewer frequency sub-channels; support T corresponds to the zero-Doppler component.

We note that around 3 ms the lowest estimation error is achieved for the 10 dB SNR case (Fig. 7) for each sampling ratio, with a total difference of ∼5.5 dB (−19 dB for 100% sampling to ∼−13.5 dB for 40% sampling) across a potential savings of 60% transmitted signal compression and corresponding energy savings. In particular, the performances between 80% and 100% sampling ratios are comparable (<2 dB drop in NMSE estimation error). We attribute this potential 20%-2 dB compression-performance trade-off to the moderately calm nature of the SPACE08 channel in question. The main channel activity is dominated by the steady-state channel components captured in the low-Doppler columns, and any transient activity manifest along the high-Doppler columns, which exhibit an extremely sparse support. Results for the five SNR case show similar characteristics with the optimal window length attained at a higher value, ∼4.61 ms, to compensate for the increase in ambient noise.

As the window length increases, we localize the channel primarily along its steady-state components and, therefore, lose accuracy of estimation along the high-Doppler columns. Hence, we observe a consistent fall in the NMSE estimation error across all sampling ratios for observation window lengths >3 ms. Thus, we conclude that robust channel estimation under energy efficient transmitted dictionaries is best achieved when the transmitted codebook *and the observation window length* sufficiently capture the underlying support of the channel across both transient and steady-state components.

So far, we have always estimated the channel with full (100%) sampling along the zero-Doppler column. We now examine the NMSE performance when we allow partial sampling along the zero-Doppler column, which captures most of the channel steady-state activity. Figure 10 shows the channel reconstruction results in terms of NMSE (in dB) with four methods of partially sampling the zero-Doppler column. We estimate the channel with 50% compressive transmission at 5 dB SNR and a window length of 3.07 ms. This implies that only half of the rows of channel matrix **U** shown in Fig. 5 are transmitted and, hence, only half of the data points of the zero-Doppler component (center column in Fig. 5) are measured or received at the receiver. We perform the experiment for 50 windows. From Fig. 5, we note that method 1 fails to reconstruct the channel because it does not fill the non-measured samples (50% samples) of the zero-Doppler component ($k \notin \Omega_s$) with any *a priori* (noisy) estimate. Since zero-Doppler components are the most dominant energy components, they are required to be sampled explicitly. Hence, this method fails to capture the channel steady-state and, therefore, performs poorly.

In method 2, all the zero-Doppler estimates of one window are used in successive windows. This method is able to reconstruct the channel with good accuracy up to a certain number of successive windows. Since the channel is time varying, channel reconstruction accuracy drops exponentially as we move farther away from the window whose estimates of zero-Doppler are used in subsequent windows. To show the variation of channel with time, we show the magnitude profile of zero-Doppler components of the post-processed received signal **U** in Fig. 9 over 250 successive

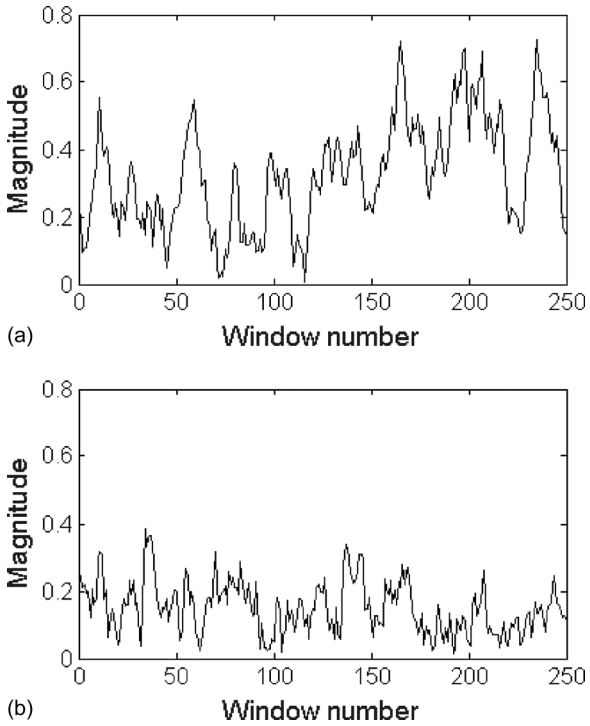

FIG. 9. (a) Magnitude profile of one data point of the zero-Doppler component measured in successive windows and having maximum variation. (b) Magnitude profile of one data point of zero-Doppler component measured in successive windows and having minimum variation.

windows. A window length of 10.75 ms is considered for Fig. 9. We show the magnitude profile of those data points of the zero-Doppler component that are having maximum and minimum variance over 250 windows in Figs. 9(a) and 9(b), respectively. Both Figs. 9(a) and 9(b) show that there is sufficient variability in the zero-Doppler component across different windows that causes method 2 to perform worse at higher window numbers.

Method 3 performs better than method 2 because, unlike method 2, all zero-Doppler components are not used from the previous window's estimate. Rather, 50% of the zero-Doppler column is directly sampled within the current window. The remaining zero-Doppler components are taken from the previous window's estimate and considered to be the noisy measurements in this window. In this method, the 50% sample *positions* of the zero-Doppler component that are measured are considered to be fixed across windows. Since the channel steady-state components are also slowly varying with time, as evident from Fig. 9, the performance of this method deteriorates similarly to method 2 as the window length increases.

Method 4 is by far the best performer and therefore, the one proposed in this work. The 50% measured samples of the zero-Doppler component are used along with the other 50% samples of the prior window's estimate. Also, the 50% sample positions are variable in successive time windows unlike method 3. This method reconstructs/estimates the channel with fairly consistent accuracy at ~ -14 dB. Also, as evident from Fig. 10, the performance of this method does not decline as the window number increases. This is primarily due to variable, rather than fixed sampling of the

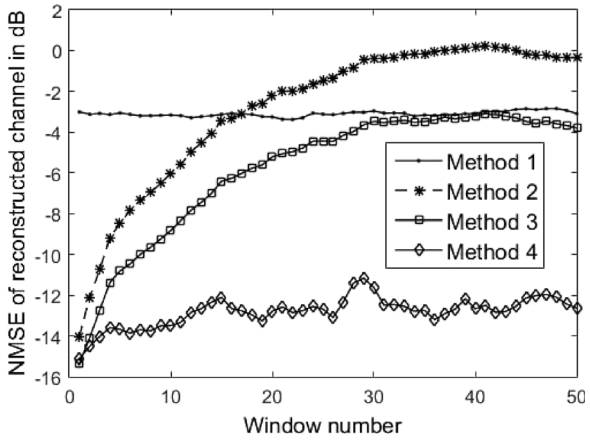

FIG. 10. NMSE for channel estimates with various methods at noisy channel SNR of 5 dB and transmission of dictionary elements over 50% frequency sub-channels at window length of 3.07 ms.

steady-state channel components along the zero-Doppler column, which captures any slow variations from one window to the next. In summary, this method is a good implementable choice in practice and, hence, can be used for energy efficient channel reconstruction when fewer dictionary elements are transmitted.

B. Results based on simulated channel

We now present similar results based on the two channels generated using the channel simulator, as discussed in Sec. I C.

We note that for the rougher channel, the performance degrades in Fig. 11 as we increase the observation window length, whereas for the calmer channel, the performance in Fig. 12 does not degrade significantly with the increasing observation window length. This is to be expected because the rougher channel, by design, has a significantly higher amount of transient activity that is poorly captured by larger observation windows. On the other hand, the calmer channel has mostly steady-state activity with few transients. Therefore, its performance does not degrade significantly when the observation window is increased. We also note that, for both the channels, the performance increases with including more Doppler columns with full measurements, e.g., compare Figs. 11(a) and 11(b), and Figs. 12(a) and 12(b). This is expected because more measurements along high-activity channel components will lead to less channel estimation errors.

Further, we note that while for both channels 100% sampling achieves the best estimation error, this performance gap (between 100% and 40% partial sampling) lessens with an increasing observation window length for both channels, with best performance achieved where the window length localizes enough steady-state components without sacrificing too much transient activity. However, as discussed above, the rough channel has more transient activity in the high-Doppler columns. This provides a mixture of high-energy components, both steady-state and transient, for the rough channel against lower-energy channel activity, which is mostly due to transient multipath reflections from

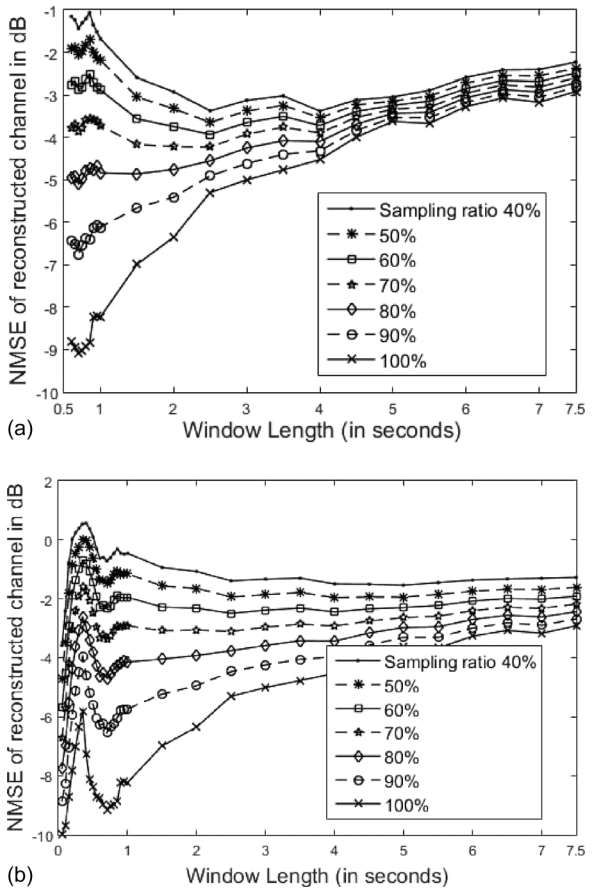

FIG. 11. Performance evaluation of calm channel (low transient channel activity) with SNR fixed at 10 dB and (a) full measurements considered along the lowest five Doppler frequencies ($-1\ Hz$, $+1\ Hz$), (b) full measurements considered along the lowest Doppler frequency 0 Hz.

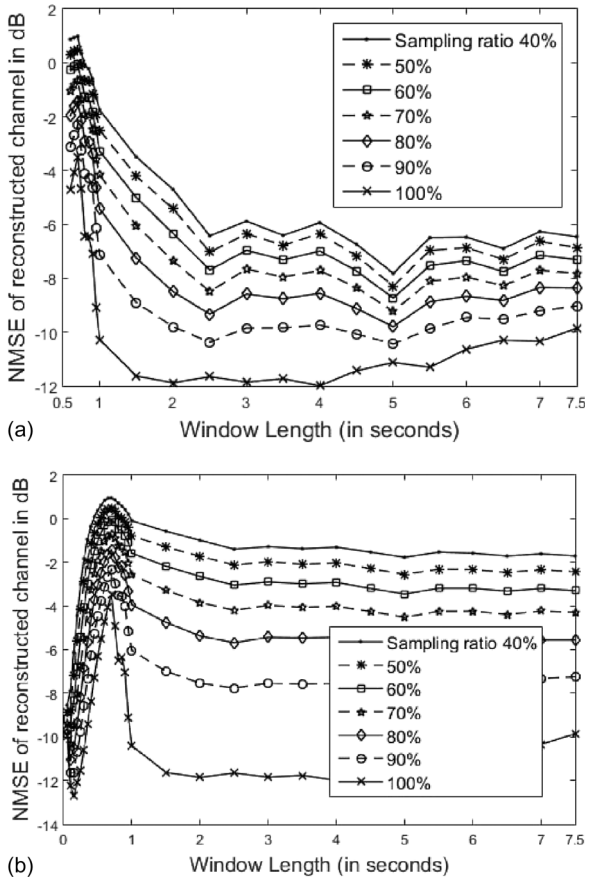

FIG. 12. Performance evaluation of calm channel (low transient channel activity) with SNR fixed at 10 dB and (a) full measurements considered along the lowest five Doppler frequencies (-1 Hz, $+1$ Hz), (b) full measurements considered along the lowest Doppler frequency 0 Hz.

multiple bounces between the ocean surface and the sea floor. On the other hand, the calmer channel has primarily high-energy channel activity that is steady-state with occasional transient multipath activity that spills over to the ± 1 Hz low-Doppler columns. In other words, the calmer channel exhibits little or no activity outside the low-Doppler activity regions, in contrast to the rough channel. This implies that sampling the calm channel using compressive sampling ratios will not necessarily lead to noise suppression and, hence, gains in performance or energy savings. On the other hand, for the rough channel, the noise suppression capability of compressive sampling captures the outlier high-Doppler transients almost leading to better overall results for the calmer channel compared to the rougher channel.

In summary, for rough channels with high-energy transient activity, full measurements at smaller observation windows (100% sampling across all Doppler columns) will be the best albeit energy-expensive strategy. However for calmer channels, i.e., with more sparse support in the high-Doppler columns, adopting compressive sampling at higher Doppler columns and a longer observation window will significantly lower the energy requirement of transmitted signals without significant decrease in estimation error. Therefore, as the channel conditions change from calm to rough or vice versa, the compressive sampling ratio and observation window can be adapted to achieve the best trade-off between transmission energy efficiency and channel estimation error.

The Appendix provides details of the simulated channels used to generate the results in Figs. 11 and 12. Figures 13–15 provide performance comparisons between the different sampling ratios as a function of scattering parameters such as the spreading factor k, intrapath variabilty S_p, as well as the bandwidth B. These parameters are explained in detail in Ref. 38 and listed in the Appendix. We observe that while full-energy (100% sampling ratio) transmission achieves the lowest NMSE error in each case, the gap in performance between different sampling ratios (and hence different rates of transmission savings) is less for the rough channel than for the calm channel. This is consistent with our earlier observations of error performance as a function of the observation window length in Figs. 12 and 13, and is explained by the fact that compressive transmission is most effective for recovering few high-energy components against a noisy background, a scenario in which the rough channel manifests much more than the calm channel. However, we observe a similar non-monotonic pattern in both channels where the performance gap between full-energy and partial-energy transmission fluctuates as a function of k, S_p, and B. Our interpretation of this fluctuating behavior is that with increased scattering there are quasi-cyclic fluctuations in

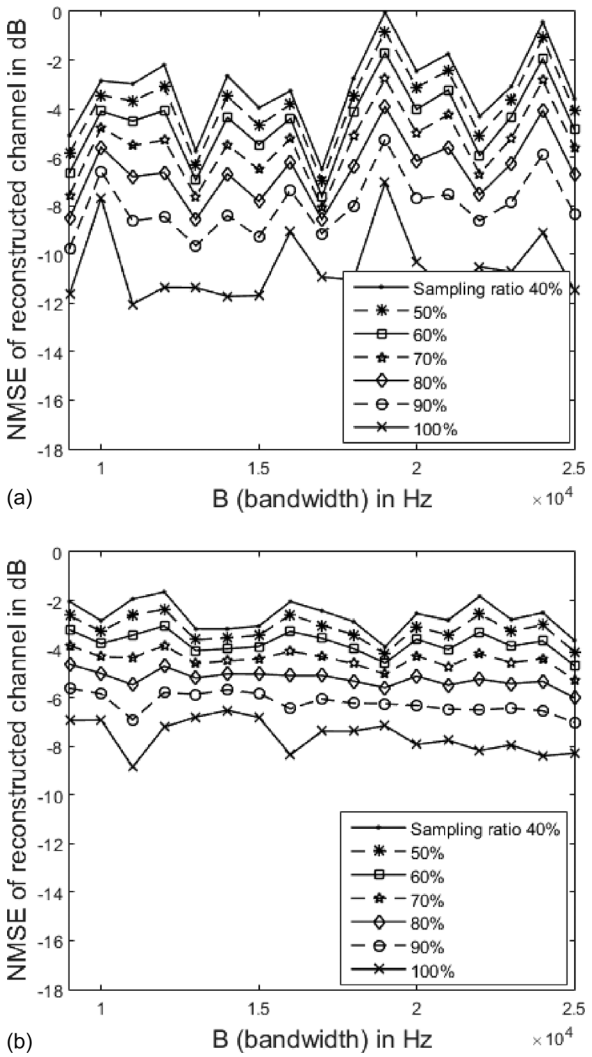

FIG. 13. NMSE vs bandwidth at window length of 30 at 10 dB SNR with five fixed Doppler for (a) calm channel and (b) rough channel.

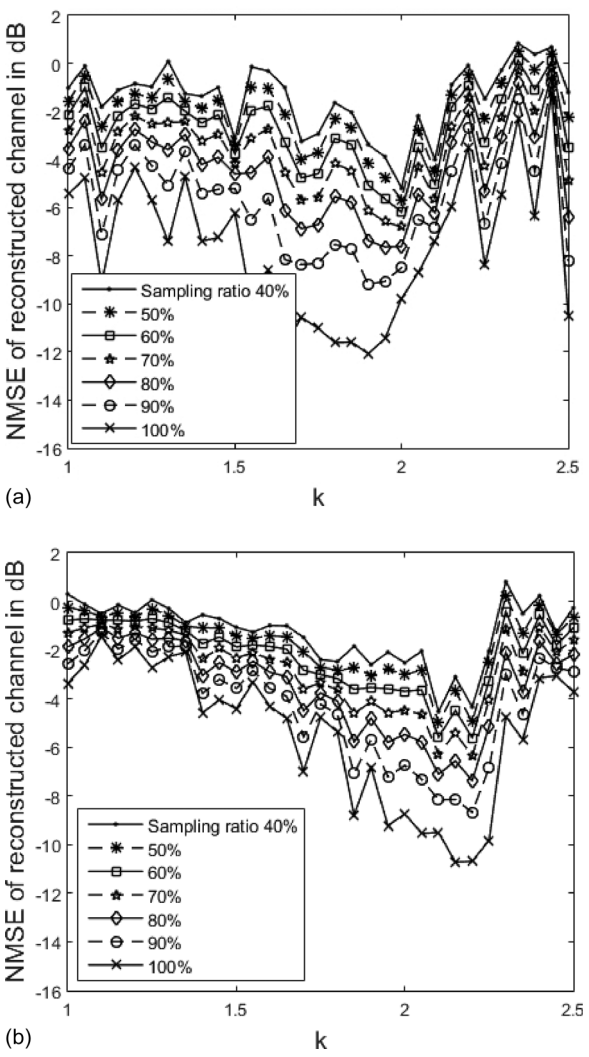

FIG. 14. NMSE vs k (spreading factor) at window length of 30 at 10 dB SNR with five fixed Doppler for (a) calm channel and (b) rough channel.

regions of constructive and destructive interference. This leads to fluctuations in the number of high-energy channel delay taps and, hence, in the sparseness of the overall channel support, sparseness being inversely proportional to the degree of constructive interference. This leads to the full-energy transmission (100% sampling) outperforming the partial energy transmissions at a higher margin whenever the sparseness decreases due to more constructive interference between the multipath and intrapath scattering events. Figure 16 shows the performance analysis of the rough channel as a function of increasing multipath arrivals P.

VI. CONCLUDING REMARKS

In this work, we aim to harness the power of compressive sampling to achieve significant savings in the number of training symbols needed to learn the sparse time-varying shallow water acoustic channel and, therefore, attain significant savings in transmission energy. This is achieved by transmitting fewer dictionary signals via compressive transmission, but employing full measurements of zero-Doppler carrying steady-state and high-energy components. The CS based framework leads to under-determined set of linear equations that would yield infinite solutions in general. Relevant assumptions, such as sparsity, allow one to retrieve a unique solution and, hence, are widely deployed along with mixed-norm solutions in CS based reconstruction. Thus, the key idea is that we need to send significantly fewer training symbols to estimate the sparse channel if we use CS rather than traditional non-sparse techniques. Thus, this work does not dismiss non-sparse techniques, but harnesses the power of compressive sampling techniques where the channel is indeed sparse and transmission energy savings can be gained. We note that sparse recovery techniques will not perform as well if the channel itself is not sparse. The scope of this work is for shallow water acoustic channels where the channel is sparse, and offers a mixture of steady-state and transient high-energy channel activity where applying CS for transmitted signal energy savings makes sense. We have shown through simulations and experimental data cases where the shallow water acoustic channel follows such meager support, particularly, along the higher Doppler columns where the transient channel phenomena are captured.

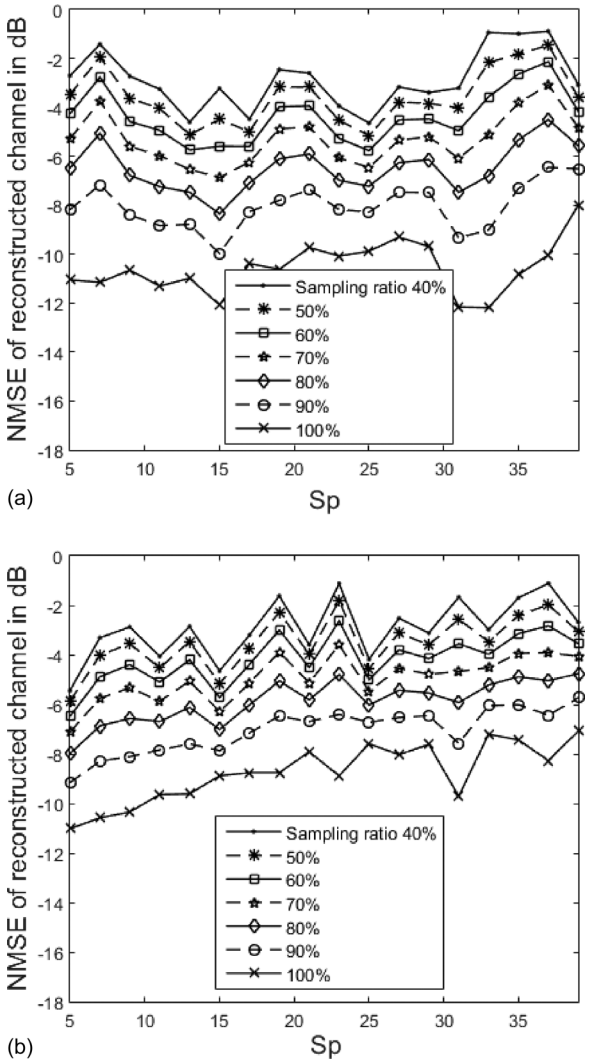

FIG. 15. NMSE vs Sp (number of intra-paths) at window length of 30 at 10 dB SNR with five fixed Doppler for (a) calm channel and (b) rough channel.

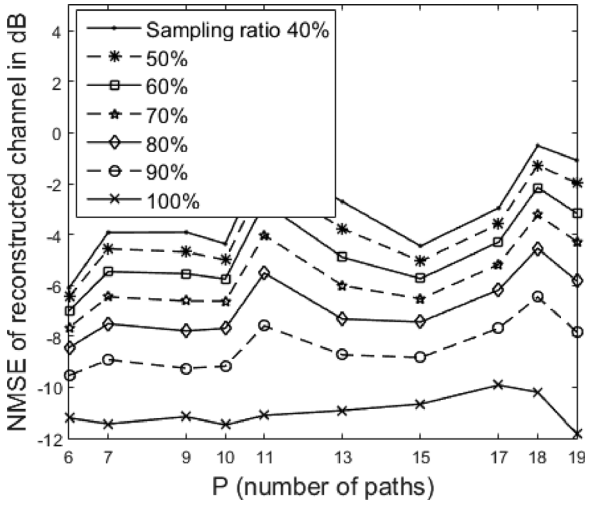

FIG. 16. NMSE vs **P** at window length of 30 at 10 dB SNR with five fixed Doppler for rough channel.

A. Key contributions

The theoretical contribution of this work is energy efficient real-time shallow water channel estimation using compressed transmission signaling. This is a significant contribution toward undersea signal processing techniques due to its potential impact across diverse underwater applications. We iterate several benefits from our proposed method below.

(i) Energy savings in transmitted signal for channel estimation can enable longer battery life for underwater communication systems, e.g., those mounted on AUVs.

(ii) Energy efficiency in the transmitted signal leads to lowered average energy of transmission in communication or surveillance systems. Low-energy channel estimation allows covert or low-presence monitoring of the ocean. For example, real-time channel knowledge enables understanding of multipath effects, which can provide crucial information regarding the nature of reflectors in the ocean, natural or anthropogenic. Besides military applications, low-presence acoustic oceanic monitoring is also highly desirable for keeping marine life safe from anthropogenic acoustic pollution of the ocean.

(iii) Energy efficient signal transmissions based on compressive transmission, such as the method presented in this work, also suppress ambient channel noise by design. This is because sparse sensing techniques are optimized toward locating the high-energy channel components, which represent the high SNR parts of the channel delay spread.

From a technical perspective our contribution toward energy efficient transmission lies in harnessing 2-D frequency localization with compressive transmission at the transmitter and modified-compressive sensing (modified-CS) with prior information at the receiver to exploit the sparse structure of the rapidly fluctuating shallow water acoustic channel in real time.

Specifically, frequency-selective transmitter dictionary design proposed in Refs. 8–10 for shallow water acoustic communications is exploited to disambiguate slowly varying channel multipath phenomena against high-energy transients, e.g., from surface wave focusing events,[1] as well as other rapidly varying oceanic events such as constructive interference between different multipath arrivals, specular reflections from moving sea surface, among others. This disambiguation of diverse types of channel effects in a frequency-selective transmission scheme allows design of independent dictionaries that pursue high-accuracy estimation of slow and fast channel multipath at different sampling rates. The proposed method is distinct in conception and structure from other frequency-selective transmission techniques designed for underwater OFDM systems[35,36] and other compressing sampling techniques that use deterministic Fourier sampling.[37] We build upon a 2-D frequency domain representation of the shallow water channel,[8] and introduce transmitter signal design in this domain that is cognizant of underwater acoustic multipath phenomena. For high-accuracy channel estimation, modified-CS with a prior

information based approach is employed. This approach is used for channel estimation in Ref. 10 also, but that work did not consider energy efficient transmission.

B. Future work

In the future, we will explore codebook design along with dictionary transmission where channel estimation and data recovery will be performed simultaneously. Despite the focus on shallow water acoustic channel estimation, the emphasis of this work is energy efficient signal processing and, therefore, may be generalizable beyond this target application. For example, one may consider energy efficient video communications where different components moving at different time rates and exhibiting different energy levels are transmitted using the non-uniform dictionary proposed in this work.

Further, UWA (underwater acoustic) communication systems requiring high power efficiency are also designed to work under robust communication modulation such as multiple frequency shift keying (MFSK) and frequency hopping spread spectrum (FHSS), which may not require channel estimation. However, channel estimation may itself be desirable to understand the ocean state at the time the communication happens, which is beyond the goal of high data-rate communications. The scope of this work is those scenarios where robust real-time channel estimation is in-itself a desirable goal for which we are not proposing any new modulation scheme, but rather an energy efficient way of transmitting the training signal that can robustly estimate and learn the channel, although one can always improve performance by using complex modulation schemes that can ride as a higher layer of abstraction on the sampling scheme used. As a future work, it will indeed be interesting to see whether adapting sophisticated modulation schemes over the non-uniform sampling gives a significant boost to the energy efficiency of the overall transmitted signal.

ACKNOWLEDGMENTS

This work was partially supported by the Council of Scientific and Industrial Research (CSIR), Government of India, and the United States Office of Naval Research, Ocean Acoustics Program, Grant No. N000141812081.

APPENDIX

Below is the list of parameters used to simulate calm and rough underwater acoustic channels used in experiments generated using,[38] with the help of MATLAB code present at[19]

Parameters for "the calm" channel

h0 = 75; [surface height (depth), m]
ht0 = 50; (transmitter height, m]
hr0 = 50; (receiver height, m)
d0 = 1000; (channel distance, m)
k = 1.9; (spreading factor)
c = 1500; (speed of sound in water, m/s)
c2 = 1200; [speed of sound in bottom, m/s (>1500 for hard, <1500 for soft)]
cut = 5; (do not consider arrivals whose strength is below that of direct arrival divided by cut)
fmin = 8.5e3; (minimum frequency, Hz)
B = 9e3; (bandwidth, Hz)
df = 25; (frequency resolution, Hz, f_vec=fmin:df:fmax;)
dt = 50 e-3; (time resolution, s)
T_SS = 60; (coherence time of the small-scale variations, s)
Small-scale (S-S) parameters:
sig2s = 2; (variance of S-S surface variations)
sig2b = sig2s/2; (variance of S-S bottom variations)
B_delp = 5 e-4; [3-dB width of the power spectral density of intra-path delays (assumed constant for all paths)]
Sp = 5; [number of intra-paths (assumed constant for all paths)]
mu_p = .5/Sp; [mean of intra-path amplitudes (assumed constant for all paths)]
nu_p = 1 e-6; [variance of intra-path amplitudes (assumed constant for all paths)]
Large-scale (L-S) parameters:
T_tot = 3*T_SS; (total duration of the simulated signal, s)
t_tot_vec=(0:dt:T_tot); Lt_tot=length(t_tot_vec);
h_bnd=[-10 10]; [range of surface height variation (L-S realizations are limited to h+h_band)]
ht_bnd=[−5 5]; (range of transmitter height variation)
hr_bnd=[−5 5]; (range of receiver height variation)
d_bnd=[−20 20]; (range of channel distance variation)
sig_h = 1; (standard deviation of L-S variations of surface height)
sig_ht = 1; (standard deviation of L-S variations of transmitter height)
sig_hr = 1; (standard deviation of L-S variations of receiver height)
sig_d = 1; (standard deviation of L-S variations of distance height)
a_AR = .9; [AR parameter for generating L-S variations (constant for variables h, ht, hr, d)]

Parameters for rough channel

h0 = 75; [surface height (depth), m]
ht0 = 50; (transmitter height, m)
hr0 = 50; (receiver height, m)
d0 = 1000; (channel distance, m)
k = 1.9; (spreading factor)
c = 1500; (speed of sound in water, m/s)
c2 = 1200; [speed of sound in bottom, m/s (>1500 for hard, <1500 for soft)]
cut = 200; (do not consider arrivals whose strength is below that of direct arrival divided by cut)
fmin = 8.5e3; (minimum frequency, Hz)
B = 9e3; (bandwidth, Hz)
df = 25; (frequency resolution, Hz, f_vec=fmin: df:fmax;)
dt = 50 e-3; (time resolution, s)
T_SS = 60; (coherence time of the small-scale variations, s)
S-S parameters:
sig2s = 10; (variance of S-S surface variations)
sig2b = sig2s/2; (variance of S-S bottom variations)
B_delp = 5 e-4; [3-dB width of the p.s.d. of intra-path delays (assumed constant for all paths)]
Sp = 40; [number of intra-paths (assumed constant for all paths)]

mu_p = .5/Sp; (mean of intra-path amplitudes [assumed constant for all paths)]
nu_p = 1 e-3; (variance of intra-path amplitudes [assumed constant for all paths)]
L-S parameters:
T_tot = 3*T_SS; (total duration of the simulated signal, s)
t_tot_vec = (0:dt:T_tot); Lt_tot=length(t_tot_vec);
h_bnd=[−10 10]; [range of surface height variation (L-S realizations are limited to h+h_band)]
ht_bnd=[−5 5]; (range of transmitter height variation)
hr_bnd=[−5 5]; (range of receiver height variation)
d_bnd=[−20 20]; (range of channel distance variation)
sig_h = 1; (standard deviation of L-S variations of surface height)
sig_ht = 1; (standard deviation of L-S variations of transmitter height)
sig_hr = 1; (standard deviation of L-S variations of receiver height)
sig_d = 1; (standard deviation of L-S variations of distance height)
a_AR = .9; [AR parameter for generating L-S variations (constant for variables h, ht, hr, d)]

[1]J. C. Preisig and G. B. Deane, "Surface wave focusing and acoustic communications in the surf zone," J. Acoust. Soc. Am. **116**(4), 2067–2080 (2004).
[2]A. S. Gupta and J. Preisig, "Tracking the time-varying sparsity of channel coefficients in shallow water acoustic communications," in *2010 Conference Record of the Forty-Fourth Asilomar Conference on Signals, Systems and Computers* (2010), pp. 1047–1049.
[3]A. S. Gupta, "Time-frequency localization issues in the context of sparse process modeling," Proc. Mtgs. Acoust. **19**(1), 070084 (2013).
[4]M. Pajovic and J. C. Preisig, "Performance analysis of the least squares based LTI channel identification algorithm using random matrix methods," in *2011 49th Annual Allerton Conference on Communication, Control, and Computing*, Allerton, IL (2011), pp. 516–523.
[5]H. Mamaghanian, N. Khaled, D. Atienza, and P. Vandergheynst, "Compressed sensing for real-time energy-efficient ECG compression on wireless body sensor nodes," IEEE Trans. Biomed. Eng. **58**(9), 2456–2466 (2011).
[6]A. Ravelomanantsoa, H. Rabah, and A. Rouane, "Simple and efficient compressed sensing encoder for wireless body area network," IEEE Trans. Instrum. Meas. **63**(12), 2973–2982 (2014).
[7]Z. Pei and Y. Wang, "Energy efficient compressed sensing of bio-signals with sparse binary matrix," in *2017 4th International Conference on Information Science and Control Engineering (ICISCE)* (July 2017), pp. 1492–1496.
[8]A. S. Gupta, N. Ansari, and A. Gupta, "Tracking the underwater acoustic channel using two-dimensional frequency sampling," in *IEEE Underwater Technology (UT)* (2015), pp. 1–5.
[9]N. Ansari, A. Gupta, and A. S. Gupta, "Physics inspired CS based underwater acoustic channel estimation," in *2015 IEEE Global Conference on Signal and Information Processing (GlobalSIP)* (2015), pp. 1106–1110.
[10]N. Ansari, A. Gupta, and A. S. Gupta, "Shallow water acoustic channel estimation using two-dimensional frequency characterization," J. Acoust. Soc. Am. **140**(5), 3995–4009 (2016).
[11]A. Sen Gupta and I. Kirsteins, "Disentangling sonar target features using braided feature graphs," In *IEEE Proc. of IEEE Oceans Conference*, Anchorage, AK (Sept. 18–21, 2017).
[12]A. Sen Gupta and R. McCarthy, "Interpreting different features of shallow water acoustic channels using braid manifolds," in *IEEE Proc. of Fourth Underwater Communications and Networking Conference (UComms)*, Lerici, Italy (August 28–30, 2018).
[13]W. Li and J. C. Preisig, "Estimation of rapidly time-varying sparse channels," IEEE J. Ocean. Eng. **32**(4), 927–939 (2007).
[14]D. L. Donoho, "For most large underdetermined systems of linear equations the minimal *l*1-norm solution is also the sparsest solution," Commun. Pure Appl. Math. **59**(6), 797–829 (2006).
[15]C. R. Berger, S. Zhou, J. C. Preisig, and P. Willett, "Sparse channel estimation for multicarrier underwater acoustic communication: From subspace methods to compressed sensing," IEEE Trans. Signal Process. **58**(3), 1708–1721 (2010).
[16]M. H. Hayes, *Statistical Digital Signal Processing and Modeling* (Wiley, New York, 1996).
[17]S. Haykin, *Adaptive Filter Theory* (Prentice-Hall, Englewood Cliffs, NJ, 2002).
[18]B. Li, S. Zhou, M. Stojanovic, L. Freitag, and P. Willett, "Multicarrier communication over underwater acoustic channels with nonuniform Doppler shifts," IEEE J. Ocean. Eng. **33**(2), 198–209 (2008).
[19]P. Qarabaqi and M. Stojanovic, "Acoustic channel modeling and simulation," 2013, available at http://millitsa.coe.neu.edu/?q=projects (Last viewed 8 April 2019).
[20]A. S. Gupta and J. Preisig, "A geometric mixed norm approach to shallow water acoustic channel estimation and tracking," Phys. Commun. **5**(2), 119–128 (2012).
[21]M. Stojanovic, J. Proakis, and J. Catipovic, "Analysis of the impact of channel estimation errors on the performance of a decision-feedback equalizer in fading multipath channels," IEEE Trans. Commun. **43**, 877–886 (1995).
[22]R. Tibshirani, "Regression shrinkage and selection via the lasso," J. R. Stat. Soc. Series B Stat. Methodol. **58**(1), 267–288 (1996).
[23]S. Song and A. C. Singer, "Blind OFDM channel estimation using FIR constraints: Reduced complexity and identifiability," IEEE Trans. Inform. Theory **53**(3), 1136–1147 (2007).
[24]M. Stojanovic, "Low complexity OFDM detector for underwater acoustic channels," in *OCEANS 2006*, Boston, MA (2006), pp. 1–6.
[25]P. C. Carrascosa and M. Stojanovic, "Adaptive channel estimation and data detection for underwater acoustic MIMO-OFDM systems," IEEE J. Ocean. Eng. **35**(3), 635–646 (2010).
[26]A. Radosevic, R. Ahmed, T. M. Duman, J. G. Proakis, and M. Stojanovic, "Adaptive OFDM modulation for underwater acoustic communications: Design considerations and experimental results," IEEE J. Ocean. Eng. **39**(2), 357–370 (2014).
[27]http://onlinelibrary.wiley.com/store/10.1002/9781118693865.app2/asset/app2.pdf?v=1&t=ie3aif1w&s=7afb39dada101981576e84176f\7f8fc09494adfa (Last viewed 8 April 2019).
[28]M. Lustig, D. L. Donoho, J. M. Santos, and J. M. Pauly, "Compressed sensing MRI," IEEE Signal Process. Mag. **25**(2), 72–82 (2008).
[29]M. Lustig, D. Donoho, and J. M. Pauly, "Sparse MRI: The application of compressed sensing for rapid MR imaging," Magn. Reson. Med.**58**(6), 1182–1195 (2007).
[30]N. Vaswani and W. Lu, "Modified-CS: Modifying compressive sensing for problems with partially known support," IEEE Trans. Signal Process. **58**(9), 4595–4607 (2010).
[31]E. van Den Berg and M. P. Friedlander, "Probing the Pareto frontier for basis pursuit solutions," SIAM J. Sci. Comput. **31**(2), 890–912 (2009).
[32]E. van den Berg and M. P. Friedlander, "SPGL1: A solver for large-scale sparse reconstruction," 2007, available at http://www.cs.ubc.ca/labs/scl/spgl1 (Last viewed 8 April 2019).
[33]M. Stojanovic, "Underwater acoustic communications: Design considerations on the physical layer," in *2008 Fifth Annual Conference on Wireless on Demand Network Systems and Services* (January 2008), pp. 1–10.
[34]P. P. J. Beaujean, "High-speed high-frequency acoustic modem for image transmission in very shallow waters," in *OCEANS 2007—Europe* (June 2007), pp. 1–6.
[35]M. Stojanovic, "Low complexity OFDM detector for underwater acoustic channels," in *IEEE OCEANS 2006* (2006), pp. 1–6.
[36]B. Li, J. Huang, S. Zhou, K. Ball, M. Stojanovic, L. Freitag, and P. Willett, "MIMO-OFDM for high-rate underwater acoustic communications," IEEE J. Ocean. Eng. **34**(4), 634–644 (2009).
[37]M. A. T. Figueiredo, R. D. Nowak, and S. J. Wright, "Gradient projection for sparse reconstruction: Application to compressed sensing and other inverse problems," IEEE J. Signal Topics Signal Process. **1**, 586–597 (2007).
[38]P. Qarabaqi and M. Stojanovic, "Statistical characterization and computationally efficient modeling of a class of underwater acoustic communication channels," IEEE J. Ocean. Eng. **38**(4), 701–717 (2013).